# Interlayer and intralayer excitons in $MoS_2/WS_2$ and $MoSe_2/WSe_2$ heterobilayers

Engin Torun,[1,*] Henrique P. C. Miranda,[1,2] Alejandro Molina-Sánchez,[3,†] and Ludger Wirtz[1]
[1]*Physics and Materials Science Research Unit, University of Luxembourg, 162a Avenue de la Faïencerie, L-1511 Luxembourg, Luxembourg*
[2]*Institute of Condensed Matter and Nanosciences (IMCN/NAPS), Universitè Catholique de Louvain, Belgium*
[3]*Institute of Materials Science (ICMUV), University of Valencia, Catedrático Beltrán 2, E-46980, Valencia, Spain*

(Received 12 March 2018; revised manuscript received 4 June 2018; published 29 June 2018)

Accurately described excitonic properties of transition metal dichalcogenide heterobilayers (HBLs) are crucial to comprehend the optical response and the charge carrier dynamics of them. Excitons in multilayer systems possess an inter- or intralayer character whose spectral positions depend on their binding energy and the band alignment of the constituent single layers. In this paper, we report the electronic structure and the absorption spectra of $MoS_2/WS_2$ and $MoSe_2/WSe_2$ HBLs from first-principles calculations. We explore the spectral positions, binding energies, and the origins of inter- and intralayer excitons and compare our results with experimental observations. The absorption spectra of the systems are obtained by solving the Bethe-Salpeter equation on top of a $G_0W_0$ calculation, which corrects the independent-particle eigenvalues obtained from density-functional theory. Our calculations reveal that the lowest energy exciton in both HBLs possess an interlayer character which is decisive regarding their possible device applications. Due to the spatially separated nature of the charge carriers, the binding energy of interlayer excitons might be expected to be considerably smaller than that of intralayer ones. However, according to our calculations, the binding energy of lowest energy interlayer excitons is only ∼20% lower due to the weaker screening of the Coulomb interaction between layers of the HBLs. Therefore, it can be deduced that the spectral positions of the interlayer excitons with respect to intralayer ones are mostly determined by the band offset of the constituent single layers. By comparing oscillator strengths and thermal occupation factors, we show that in luminescence at low temperature, the interlayer exciton peak becomes dominant, while in absorption it is almost invisible.

DOI: 10.1103/PhysRevB.97.245427

## I. INTRODUCTION

Single-layer transition metal dichalcogenides (TMDs) are two-dimensional materials that stand out due to their strong light-matter interaction and remarkable excitonic effects on the optical properties [1–4]. The assembly of multilayer structures out of these single layers is a promising direction to combine the physical properties of them for the design of a new generation of optical devices. Different stackings of 2D materials lead to different band alignments, which allows us to design the charge transfer properties upon optical excitation by choosing suitable 2D heterostructures [5–13].

Multilayer systems offer the possibility for the formation of interlayer excitons besides the intralayer ones [14–23]. This makes TMD-based heterobilayers (HBLs) potential candidates for ultrafast charge transfer [24], ultrafast formation of hot interlayer excitons [25], interlayer energy transfer [26], valleytronics [27,28], charge transfer [29–36], and long-lived interlayer excitons [37]. In addition, recent efforts have described the role of the Moiré patterns in TMD HBLs on the binding energy of excitons [38].

On the theoretical side, efforts have focused on the electronic structure, predicting the type-II alignment for several stacking combinations of TMDs using density-functional theory (DFT) calculations [14–20,39]. For the compounds with type-II band alignment, on the independent particle level, the interlayer transition is the lowest energy transition due to the band offset of the constituent single layers. However, excitonic effects might reverse the order of intra- versus interlayer transitions.

The reason is that the spectral position of the interlayer excitons with respect to intralayer ones depends not only on the band alignment but also on the excitonic binding energy, which is strongly enhanced in 2D materials (as compared to bulk materials). The exciton binding energy depends on the distance between charge carriers via the screened Coulomb interaction. As the electron and hole of the interlayer excitons are spatially separated, the binding energy of them is, *a priori,* weaker than that of intralayer ones. At the same time, however, it is known (for bulk layered systems) that the screening in the perpendicular direction is weaker than the screening in the layer plane, which in turn, tends to enhance the binding energy of interlayer excitons. If the binding energy of the interlayer exciton is much smaller than the lowest intralayer one, the band alignment with the inclusion of excitonic effects might deviate from the electronic band alignment of the compound. Therefore, the understanding of the optical response and the carrier dynamics of TMD HBLs requires an accurate calculation of the excitonic states together with the GW correction of the electronic structure.

In this paper, we report the electronic structure and optical absorption spectra, including excitonic effects and full spinorial wave functions, of $MoS_2/WS_2$ and $MoSe_2/WSe_2$ HBLs

*engin.torun@uni.lu
†alejandro.molina@uv.es

 

in the AA′ stacking configuration of them. We classify the intralayer and interlayer excitons and report the valence and conduction band alignments. We find that the lowest energy exciton of both HBLs has interlayer character (charge transfer state), which makes these systems suitable to host excitons with long lifetimes. We find good agreement with the spectral ordering of excitonic peaks in the recent photoluminescence (PL) measurements of the $MoSe_2/WSe_2$ bilayer by Wilson *et al.* [40].

## II. METHODS

We calculate the excitonic states and the optical absorption spectra of $MoS_2/WS_2$ and $MoSe_2/WSe_2$ HBLs using *ab initio* many-body perturbation theory with the Bethe-Salpeter equation (BSE) [41–43]. In this formalism, the excitations are expressed in terms of electron-hole pairs:

$$(E_{c\mathbf{k}} - E_{v\mathbf{k}})A^S_{vc\mathbf{k}} + \sum_{\mathbf{k}'v'c'} \langle vc\mathbf{k}|K_{eh}|v'c'\mathbf{k}'\rangle A^S_{v'c'\mathbf{k}'} = \Omega^S A^S_{vc\mathbf{k}}, \tag{1}$$

where $E_{c\mathbf{k}}$ and $E_{v\mathbf{k}}$ are the quasiparticle energies of the valence and the conduction band states, respectively. The energies and wave functions are obtained from DFT as implemented in QUANTUM ESPRESSO [44] using the local density approximation (LDA) and norm-conserving fully relativistic pseudopotentials [45]. The pseudopotentials are generated based on the parameters of PSEUDODOJO [46]. The plane-wave energy cutoff in the ground-state calculations is set to 120 Ry. We use fully relativistic pseudopotentials; semicore electrons for Mo (4s and 4p) and W (4d, 5s, and 5p) are treated as valence states in the calculations. The vacuum distance between two periodic images is approximately 40 a.u. for both the single and bilayers. To get the quasiparticle eigenvalues, the LDA energies are corrected by the $G_0W_0$ approximation [47,48], as implemented in the Yambo code [49]. The $G_0W_0$ quasiparticle energies are calculated on a $42 \times 42 \times 1$ **k**-grid, centered on Γ. We use 160 bands for the self-energy and 160 bands for the dynamical dielectric screening.

The $A^S_{vc\mathbf{k}}$ are the expansion coefficients of the excitonic states and $\Omega^S$ are their energies. The interaction kernel between electrons and holes, $K_{eh}$, contains the unscreened exchange interaction $V$ (repulsive) and the screened direct Coulomb interaction (attractive) $W$. The latter term $W$ depends on the dielectric screening. In the case of 2D materials, the accurate treatment of the dielectric screening is crucial. The lower dielectric screening (when compared with 3D materials) results in large exciton binding energies, of the order of 0.5 eV [50–52].

The imaginary part of the dielectric function, $\epsilon(\hbar\omega) = \epsilon_1(\hbar\omega) + i\epsilon_2(\hbar\omega)$, is proportional to the optical absorption spectra. It is expressed, in terms of the excitonic states, as

$$\epsilon_2(\hbar\omega) \propto \sum_S \left| \sum_{cv\mathbf{k}} A^S_{vc\mathbf{k}} \frac{\langle c\mathbf{k}|p_i|v\mathbf{k}\rangle}{(\epsilon_{c\mathbf{k}} - \epsilon_{v\mathbf{k}})} \right|^2 \delta(\Omega^S - \hbar\omega), \tag{2}$$

where $\langle c\mathbf{k}|p_i|v\mathbf{k}\rangle$ are the dipole matrix elements of transitions from the valence to the conduction bands. We consider in-plane polarization for both single- and bilayers. The out-of-plane absorption gives a negligible contribution at the band gap energies due to depolarization effects. To mimic the experimental results, the delta function is replaced by a Lorentzian with 0.05 eV broadening. Similar to $G_0W_0$, the BSE calculations are also performed using the Yambo code with Γ centered $42 \times 42 \times 1$ **k**-grid [49]. To avoid the long-range interaction between the periodic copies of the single layer along the vertical direction, a Coulomb cutoff of the screened potential is used in both $G_0W_0$ and BSE calculations. Since we are dealing only with the low-energy part of the absorption spectra, it is sufficient to include only the four highest valence bands and four lowest conduction bands in the Bethe-Salpeter kernel. Our systematic convergence study shows that the mentioned settings (number of bands and **k**-points) are required to get 50 meV convergence of the $G_0W_0$ band gap and the excitonic peaks in the BSE spectra.

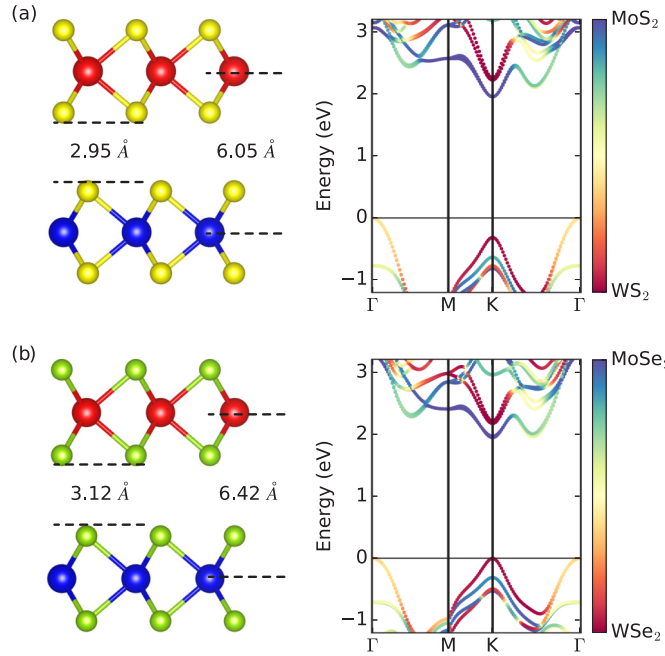


FIG. 1. Optimized atomic and projected electronic structures of (a) $MoS_2/WS_2$ and (b) $MoSe_2/WSe_2$ HBLs. The red, blue, yellow, and light green atoms correspond to W, Mo, S, and Se, respectively.

## III. RESULTS

The lattice parameters of $MoS_2$ ($MoSe_2$) and $WS_2$ ($WSe_2$) single layers are almost commensurate [18,53], which justifies the construction of the HBLs assuming AA′ stacking [see the geometries in Fig. 1(a)] with the bulk lattice parameters of 3.162 Å and 3.288 Å for $MoS_2/WS_2$ and $MoSe_2/WSe_2$ HBLs, respectively [54]. In our ground state calculations, we use these experimental lattice parameters without performing further optimization but we have relaxed the atomic positions and the distance between layers on the LDA level. Even though the LDA completely neglects the van der Waals interaction between layers, it gives reasonable interlayer distances for many layered systems because it overestimates the weak covalent contribution to the interlayer bonding [51].

### A. Orbital-projected band structure

Even without calculating the optical properties, the electronic structure of the HBLs already offers valuable information. Figures 1(a) and 1(b) show the band structures of $MoS_2/WS_2$ and $MoSe_2/WSe_2$ HBLs, respectively. The bands in the figure are projected onto the atomic orbitals of the single layers. Therefore, bands with blue and red colors correspond to $MoS_2$ ($MoSe_2$) and $WS_2$ ($WSe_2$) layers, respectively.

As can be seen in Fig. 1, the conduction and valence bands at the K point in the Brillouin zone (BZ) are not hybridized and can be assigned unambiguously to the constituent single layers. The trend is that the conduction band minima are purely localized on the $MoX_2$ whereas the valence band maxima are localized on the $WX_2$ layers where X represents S and Se atoms. Therefore, on the LDA level, the band alignment of HBLs are type-II, with conduction band (electrons) and valence band (holes) located at different layers. The $G_0W_0$ calculations change the magnitude of the alignments but not the character. Moreover, the order of the valence band states is determined by including properly the spin-orbit interaction. In our calculations, the spin-orbit interaction is included exactly using full spinor wave functions. Table I reports the values of band gaps, band offsets, and spin-orbit splitting, as obtained in LDA and $G_0W_0$ levels. It is important to note that there is some uncertainty in the absolute GW band-gap values of single- and bilayer TMDs, depending on the approximation. For instance, for single-layer $MoS_2$, the value ranges from 2.40 to 2.75 eV [51]. As can be seen in the table, our values for single- and bilayer configurations reside in the lower region of the GW gap span of each compound. What is important, however, is the relative position of intra- and interlayer excitons.

In addition, the interlayer interaction makes the HBLs indirect semiconductors on both the LDA and the $G_0W_0$ level.

TABLE I. Direct LDA and $G_0W_0$ energy gap, SOC splitting, and band offset at the point K in the BZ of the $MoS_2/WS_2$ and $MoSe_2/WSe_2$ HBLs and constitute single layers. VB and CB stands for valence and conduction band, respectively. The band offset values in $G_0W_0$ are shown in parantheses.

| | Energy Gap (eV) | | SOC splitting (eV) | Band offset (eV) | |
|---|---|---|---|---|---|
| | LDA | $G_0W_0$ | | VB | CB |
| $MoS_2$ | 1.62 | 2.54 | 0.16 | – | – |
| $WS_2$ | 1.56 | 2.52 | 0.45 | – | – |
| $MoS_2/WS_2$ | 1.29 | 2.26 | – | 0.32(0.22) | 0.27(0.23) |
| $MoSe_2$ | 1.38 | 2.19 | 0.20 | – | – |
| $WSe_2$ | 1.30 | 2.23 | 0.49 | – | – |
| $MoSe_2/WSe_2$ | 1.07 | 1.95 | – | 0.31(0.24) | 0.21(0.19) |

As shown in Fig. 1, the valence band maximum is located at Γ and composed of hybrid orbitals from both layers. The conduction band minimum is located at the K point and composed of nonhybridized Mo orbitals. Our calculations also show that $MoS_2/WS_2$ and $MoSe_2/WSe_2$ are indirect band gap semiconductors with a LDA ($G_0W_0$) gap of 1.10 (1.92) and 1.05 (1.74) eV, which is consistent with the results for HBL systems [17].

### B. Optical spectra

In layered compounds, excitonic effects are much stronger than in bulk compounds due to reduced Coulomb screening. The prominent excitonic effects are particularly important for the low-energy optical response and the charge carrier dynamics of the ultrathin materials. In the case of HBLs, the

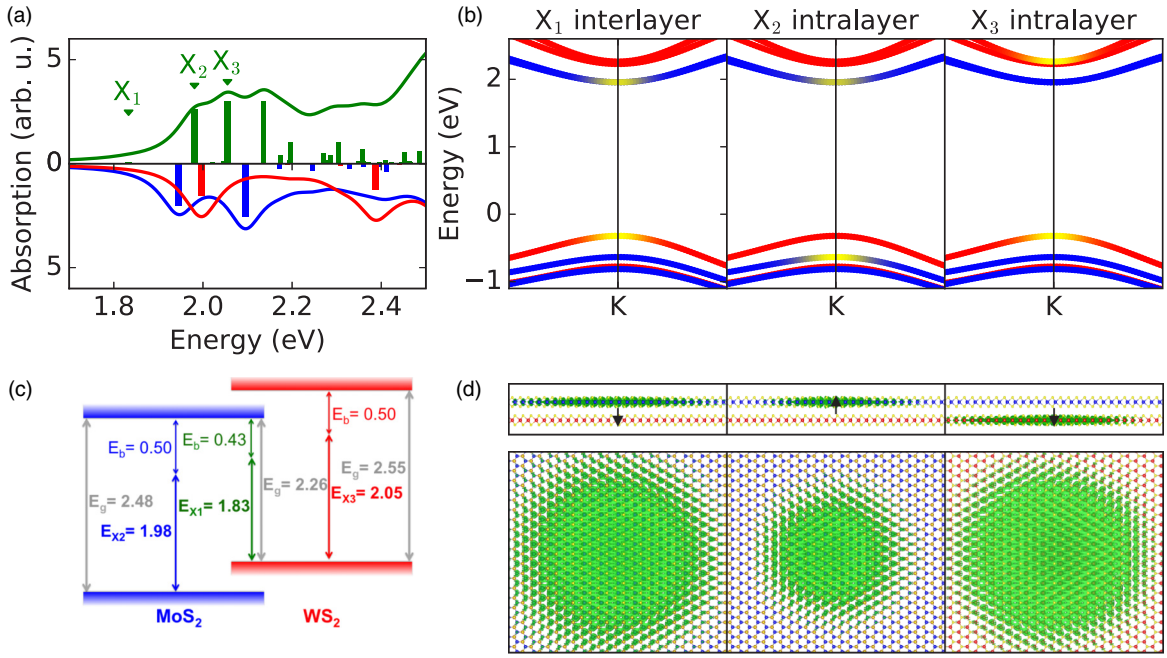


FIG. 2. Optical absorption spectra of (a) $MoS_2/WS_2$ and constituent single layers (blue and red curves for Mo and W compound, respectively). (b) Electronic bands near the K point in the BZ with the transitions contributing to the exciton. (c) Band alignment of the HBLs with excitonic effects. (d) The charge density of the indicated excitons with a fixed hole position marked with a black arrow.

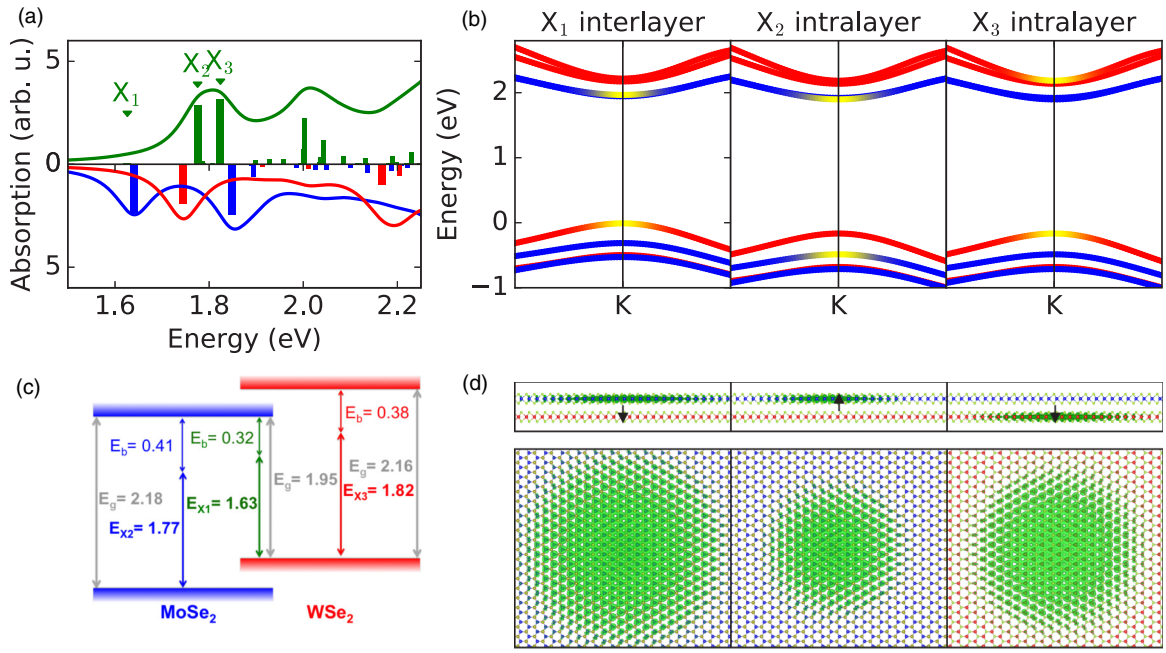


FIG. 3. Optical absorption spectra of (a) $MoSe_2/WSe_2$ and constituent single layers (blue and red curves for Mo and W compound, respectively). (b) Electronic bands near the K point in the BZ with the transitions contributing to the exciton. (c) Band alignment of the HBLs with excitonic effects. (d) The charge density of the indicated excitons with a fixed hole position marked with a black arrow.

excitons might have inter- or intralayer character depending on their band composition. The spectral positions of these excitons depend on their binding energies and the band alignment of the constituent single-layers. Therefore, the type-II band alignment of the HBLs obtained in the independent-particle picture can be insufficient to ensure an interlayer exciton at the lowest energy in the optical spectra. Thus, a realistic calculation of excitonic binding energies and a characterization of the optical properties of TMD HBLs demands accurate *ab initio* methods with the BSE approach, including the spin-orbit coupling.

The optical spectra including excitonic effects of $MoS_2/WS_2$ and $MoSe_2/WSe_2$ HBLs are shown in Figures 2 and 3, respectively. In both figures, panel (a) shows the absorption spectra for the constituent layers $MoX_2$ (blue), $WX_2$ (red), and HBLs (green). We focus on the absorption threshold of the spectra, in particular on the first three bright excitons of each HBL.

In the case of $MoS_2/WS_2$ HBL, the $X_1$ exciton is an interlayer exciton, which is energetically lower than the intralayer ones as shown in Fig. 2(a). The projected band structure [Fig. 2(b)] shows that the exciton is composed of transitions from the top of the highest valence band at K to the minimum of the second conduction band (note that the spin-orbit splitting of the conduction band minimum is only 3 meV [55] and thus the two lowest conduction bands cannot be distinguished on the energy scale of Fig. 2). The exciton wave function is represented by fixing the hole and plotting the electron density. In all the figures, the maximum of the electron density is set to 1 and we fix a consistent isosurface value. The electronic part of the wave function of the $X_1$ exciton localizes in the $MoS_2$ layer when the hole is placed in the $WS_2$ layer, which clearly indicates the charge-separated feature of the interlayer $X_1$ exciton, as can be see in Fig. 2(d) [56]. The small oscillator strength of this exciton peak is the result of the spatially separated charge carriers. Another important point is that the interlayer $X_1$ exciton is not the lowest energy exciton in the absorption spectrum of the HBL. There is another interlayer exciton, $X_0$, almost dark, and 3 meV lower in energy. The interlayer $X_0$ exciton comes from direct transitions from valence to conduction band at K. They small oscillator strength is exclusively related to the even symmetry of the exciton (see Ref. [57] for an extended discussion). Therefore, PL can be quenched at low temperatures if the splitting $X_0 - X_1$ is large enough (as noted already for PL from intralayer excitons [55,58]).

In addition to the interlayer exciton, we also present the first two intralayer excitons derived from band-to-band transitions within each single-layer. It can be seen in the projected band structure plot that the intralayer excitons $X_2$ and $X_3$ belong to $MoS_2$ and $WS_2$ layers, respectively. The localization of the electron and the hole in the same layer [see Fig. 2(d)] enhances the oscillator strength and therefore the absorption is much stronger than for the interlayer exciton. These excitons are slightly redshifted with respect to the single-layer excitons [see blue and red spectra in Fig. 2(a)], as a result of the increased dielectric screening in the case of bilayer.

The excitonic binding energies of the HBLs provide valuable information of their optical properties. Table II shows that the interlayer exciton, $X_1$, of $MoS_2/WS_2$ HBL has a binding energy of 0.43 eV, which is 70 meV smaller than that of the first intralayer exciton, $X_2$, originating from the $MoS_2$ layer. This is an expected outcome since the charge carriers of interlayer excitons are spatially separated which reduces the binding energy. Yet, the weaker Coulomb screening between layers prevents the binding energy of the interlayer excitons from

TABLE II. The spectral position, composition, and binding energy of the excitons indicated in Fig. 1. We include the peak positions of the $X_2$ and $X_3$ excitons in the parentheses in the case of single layer.

| | $MoS_2/WS2$ | | | | $MoSe_2/WSe2$ | | | |
|---|---|---|---|---|---|---|---|---|
| | $X_0$ | $X_1$ | $X_2$ | $X_3$ | $X_0$ | $X_1$ | $X_2$ | $X_3$ |
| Spectral position (eV) | 1.830 | 1.833 | 1.98 (1.95) | 2.05 (1.99) | 1.60 | 1.63 | 1.77 (1.64) | 1.82 (1.75) |
| Binding energy (eV) | 0.43 | 0.43 | 0.50 | 0.50 | 0.32 | 0.32 | 0.41 | 0.38 |
| Composition | W-Mo | W-Mo | Mo-Mo | W-W | W-Mo | W-Mo | Mo-Mo | W-W |

being much smaller than the binding energy of the intralayer ones. The competition of these two contributions together with the large band offset ultimately leads to a sufficiently large binding energy such that the interlayer exciton is the lowest energy one. Therefore, the optical properties of a $MoS_2/WS_2$ HBL correspond to the ones of a type-II heterostructure in spite of the strong excitonic effects of 2D materials. Note, however, that the difference in excitonic effects reduces the energy difference between inter- and intralayer exciton to 150 meV as opposed to an energy difference of 260 meV that would be expected in the independent-particle model (neglecting excitonic binding energy). It is worth it to mention that high accuracy of first-principles calculations is required to obtain a reliable result. The omission of the spin-orbit interaction (up to 0.5 eV for $WS_2$) and/or of the Coulomb cutoff can dramatically change the result and the conclusions.

Regarding the $MoSe_2/WSe_2$ HBL, the analysis of Fig. 3 gives similar physical conclusions but some quantitative differences. The binding energies are smaller than that of the previous case, i.e., the binding energies of interlayer and intralayer excitons are 0.32 eV and 0.41 eV, respectively. Similar to the previous case, the $MoSe_2/WSe_2$ HBL displays the character of type-II band alignment, both on the independent-particle level and when excitonic effects are included. In addition, the $X_0$ exciton (30 meV below the $X_1$!) can be be clearly distinguished from the band structure shown in Fig. 3(b) for exciton $X_1$. We expect the effect of PL quenching to be more visible at low temperature for $MoSe_2/WSe_2$ HBL than in the case of $MoS_2/WS_2$.

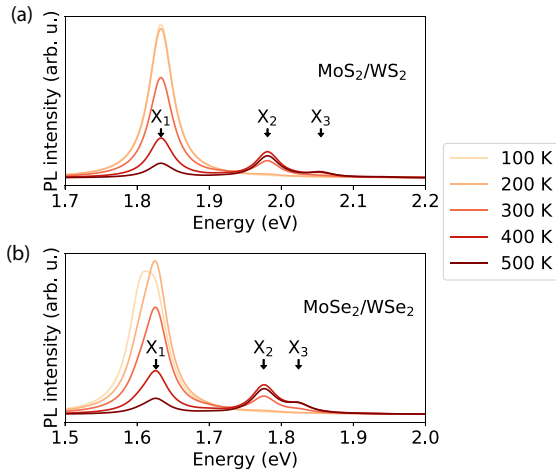


FIG. 4. Visualization of the photoluminescence intensity for the $MoS_2/WS_2$ and $MoSe_2/WSe_2$ systems in panels (a) and (b), respectively, obtained by multiplying the oscillator strength by the Bose-Einstein distribution $(e^{E_s/k_bT}-1)^{-1}$ for different temperatures where $E_s$ is the energy of the exciton. In panel (b), for temperature below 100 K the presence of the almost dark exciton $X_0$ becomes visible.

Experimental proofs of the existence of interlayer excitons are more robust for the Se-HBL than for the S-HBL case. In PL experiments, e.g., Wilson *et al.* [40] detected the intralayer exciton peaks at 1.57 and 1.64 eV for $MoSe_2$ and $WSe_2$, respectively (in qualitative agreement with our results in Table II) and the interlayer exciton around 0.22 eV below the $X_2$, in comparison with our prediction of 0.14 eV. Differences can be due to the presence of a substrate, which is neglected in our calculations and due to the bilayer twist or stacking that results from the layer depositions in the experiments. Time-dependent PL showed long lifetime excitons with low radiative efficiency, indicating that the lowest energy exciton has interlayer character in agreement with our results [58]. We present only calculations of absorption spectra where the intensity of the peaks is directly given by the dipole matrix elements (oscillator strengths) of the excitonic states [see Eq. (2)]. For the Se HBL, the oscillator strength of the interlayer exciton is 50 times smaller than the one of the lowest intralayer exciton (due to the spatial separation of the wave functions on neighboring layers). As can be seen in Fig. 3(a), the intralayer exciton can hardly be detected in an absorption experiment. In PL experiments, however, the intensity ratio of the peaks is reversed. The intensity is proportional to the oscillator strength and to the exciton population. Since the exciton recombination time is slower than the thermalization [37,59–61], we assume on a first approximation that the occupation of the excitonic states follows the Bose-Einstein distribution. Figure 4 shows a visualization the PL intensity for several temperatures, obtained by multiplying the oscillator strength by the Bose-Einstein distribution. The intensity ratio between two peaks is then modified roughly by the Boltzmann factor $\exp(-\Delta E/k_BT)$, where $\Delta E$ is the energy difference between two excitons. An improved quantitative calculation of luminescence spectra would include the transition rates from the intralayer excitons (into which absorption takes place) to the interlayer exciton. However, these rates are currently still unknown. A formal theoretical treatment of the PL can be found in Ref. [62] but is beyond the scope of the present work.

## IV. CONCLUSIONS

Our first-principles investigation on the excitons of $MoS_2/WS_2$ and $MoSe_2/WSe_2$ HBLs predict the existence of interlayer excitons, 0.15 eV and 0.24 eV below the absorption onset of intralayer excitons. This indicates that the excitonic

ground states of these systems naturally separate the electron and the hole in different layers, making TMD HBLs efficient materials for charge separation applications. We also observe that the lowest energy exciton of both HBLs, $X_0$, has a very small oscillator strength (almost dark), with a remarkable splitting of 30 meV with respect to the first bright interlayer exciton in $MoSe_2/WSe_2$ bilayer. Our calculations agree well with available experimental data [37,40] within the limits imposed by the uncertainties about heterostructure geometry (e.g., twisting angle) and influence of the substrate via screening effects. We also obtain good agreement with recently reported calculations for the $MoS_2/WS_2$ and $MoSe_2/WSe_2$ HBLs [63]. In a very recent article by Gillen *et al.*, it has been shown that the oscillator strengths but not the binding energies of the inter-layer (spatially indirect) excitons are greatly influenced by the stacking order of the HBLs [64,65]. Due to the change in the symmetry properties of the bilayer, the first inter-layer exciton which is "almost bright" in the case of the current AA′ (H) stacking becomes "almost dark" for the in-plane polarization direction in the AB (R) stacking, which can also be experimentally realized. For both bilayer systems, the dipole oscillator strength of the interlayer exciton is 50 times smaller than that of the intralayer ones. This means that in the absorption spectra, the corresponding peak is practically invisible. In luminescence spectra, however, it becomes the dominant peak. The quantitative description of the measured luminescence spectra at room temperature [40] and at 20 K [37] requires the calculation of transition rates from the intra- to the interlayer excitonic states, which is the subject of future work.

## ACKNOWLEDGMENTS

The authors acknowledge support by the Luxembourg National Research Fund, Luxembourg, through Projects INTER/ANR/13/20/NANOTMD (E.T and L.W.), C14/MS/773152/FAST-2DMAT (A.M.S.), and OTPMD (H.P.C.M.). Furthermore, A.M.S acknowledges the Juan de la Cierva (Grant IJCI-2015-25799) program (MINECO,Spain). H.P.C.M acknowledges support from the F.R.S.-FNRS through the PDR Grant HTBaSE (T.1071.15). The simulations were done using the HPC facilities of the University of Luxembourg [66]. We acknowledge stimulating discussion with Jens Kunstmann who raised the question of the relatively large binding energy of the interlayer exciton during the presentation of our work at the Flatlands 2017 conference in Lausanne. We also acknowledge Fulvio Paleari for discussion on PL intensities as a function of temperature.

[1] K. F. Mak, C. Lee, J. Hone, J. Shan, and T. F. Heinz, Phys. Rev. Lett. **105**, 136805 (2010).
[2] A. Splendiani, L. Sun, Y. Zhang, T. Li, J. Kim, C.-Y. Chim, G. Galli, and F. Wang, Nano Lett. **10**, 1271 (2010).
[3] L. Britnell, R. M. Ribeiro, A. Eckmann, R. Jalil, B. D. Belle, A. Mishchenko, Y.-J. Kim, R. V. Gorbachev, T. Georgiou, S. V. Morozov, A. N. Grigorenko, A. K. Geim, C. Casiraghi, A. H. C. Neto, and K. S. Novoselov, Science **340**, 1311 (2013).
[4] O. Lopez-Sanchez, D. Lembke, M. Kayci, A. Radenovic, and A. Kis, Nat. Nano **8**, 497 (2013).
[5] A. K. Geim and I. V. Grigorieva, Nature **499**, 419 (2013).
[6] R. Frisenda, E. Navarro-Moratalla, P. Gant, D. Perez De Lara, P. Jarillo-Herrero, R. V. Gorbachev, and A. Castellanos-Gomez, Chem. Soc. Rev. **47**, 53 (2018).
[7] M. Yankowitz, J. Xue, D. Cormode, J. D. Sanchez-Yamagishi, K. Watanabe, T. Taniguchi, P. Jarillo-Herrero, P. Jacquod, and B. J. LeRoy, Nat. Phys. **8**, 382 (2012).
[8] W. J. Yu, Y. Liu, H. Zhou, A. Yin, Z. Li, Y. Huang, and X. Duan, Nat. Nano **8**, 952 (2013).
[9] C.-H. Lee, G.-H. Lee, A. M. van der Zande, W. Chen, Y. Li, M. Han, X. Cui, G. Arefe, C. Nuckolls, T. F. Heinz, J. Guo, J. Hone, and P. Kim, Nat. Nano **9**, 676 (2014).
[10] M. M. Furchi, A. Pospischil, F. Libisch, J. Burgdörfer, and T. Mueller, Nano Lett. **14**, 4785 (2014).
[11] R. Cheng, D. Li, H. Zhou, C. Wang, A. Yin, S. Jiang, Y. Liu, Y. Chen, Y. Huang, and X. Duan, Nano Lett. **14**, 5590 (2014).
[12] F. Withers, O. Del Pozo-Zamudio, A. Mishchenko, A. P. Rooney, A. Gholinia, K. Watanabe, T. Taniguchi, S. J. Haigh, A. K. Geim, A. I. Tartakovskii, and K. S. Novoselov, Nat. Mater. **14**, 301 (2015).
[13] U. Wurstbauer, B. Miller, E. Parzinger, and A. W. Holleitner, J. Phys. D **50**, 173001 (2017).
[14] C. Gong, H. Zhang, W. Wang, L. Colombo, R. M. Wallace, and K. Cho, Appl. Phys. Lett. **103**, 053513 (2013).
[15] J. Kang, S. Tongay, J. Zhou, J. Li, and J. Wu, Appl. Phys. Lett. **102**, 012111 (2013).
[16] H. Terrones, F. López-Urías, and M. Terrones, Sci. Rep. **3**, 1549 (2013).
[17] K. Kośmider and J. Fernández-Rossier, Phys. Rev. B **87**, 075451 (2013).
[18] H.-P. Komsa and A. V. Krasheninnikov, Phys. Rev. B **88**, 085318 (2013).
[19] E. Torun, H. Sahin, and F. M. Peeters, Phys. Rev. B **93**, 075111 (2016).
[20] M. Yagmurcukardes, E. Torun, R. T. Senger, F. M. Peeters, and H. Sahin, Phys. Rev. B **94**, 195403 (2016).
[21] B. Miller, A. Steinhoff, B. Pano, J. Klein, F. Jahnke, A. Holleitner, and U. Wurstbauer, Nano Lett. **17**, 5229 (2017).
[22] T. Galvani, F. Paleari, H. P. C. Miranda, A. Molina-Sánchez, L. Wirtz, S. Latil, H. Amara, and F. Ducastelle, Phys. Rev. B **94**, 125303 (2016).
[23] H. P. C. Miranda, S. Reichardt, G. Froehlicher, A. Molina-Sánchez, S. Berciaud, and L. Wirtz, Nano Lett. **17**, 2381 (2017).
[24] X. Hong, J. Kim, S.-F. Shi, Y. Zhang, C. Jin, Y. Sun, S. Tongay, J. Wu, Y. Zhang, and F. Wang, Nat. Nano **9**, 682 (2014).
[25] H. Chen, X. Wen, J. Zhang, T. Wu, Y. Gong, X. Zhang, J. Yuan, C. Yi, J. Lou, P. M. Ajayan, W. Zhuang, G. Zhang, and J. Zheng, Nat. Commun. **7**, 12512 (2016).
[26] D. Kozawa, A. Carvalho, I. Verzhbitskiy, F. Giustiniano, Y. Miyauchi, S. Mouri, A. H. Castro Neto, K. Matsuda, and G. Eda, Nano Lett. **16**, 4087 (2016).
[27] J. R. Schaibley, H. Yu, G. Clark, P. Rivera, J. S. Ross, K. L. Seyler, W. Yao, and X. Xu, Nat. Rev. Mater. **1**, 16055 (2016).
[28] A. Molina-Sánchez, D. Sangalli, L. Wirtz, and A. Marini, Nano Lett. **17**, 4549 (2017).

[29] H. Fang, C. Battaglia, C. Carraro, S. Nemsak, B. Ozdol, J. S. Kang, H. A. Bechtel, S. B. Desai, F. Kronast, A. A. Unal, G. Conti, C. Conlon, G. K. Palsson, M. C. Martin, A. M. Minor, C. S. Fadley, E. Yablonovitch, R. Maboudian, and A. Javey, Proc. Natl. Acad. Sci. **111**, 6198 (2014).

[30] Y. Gong, J. Lin, X. Wang, G. Shi, S. Lei, Z. Lin, X. Zou, G. Ye, R. Vajtai, B. I. Yakobson, H. Terrones, M. Terrones, B. Tay, J. Lou, S. T. Pantelides, Z. Liu, W. Zhou, and P. M. Ajayan, Nat. Mater. **13**, 1135 (2014).

[31] S. Tongay, W. Fan, J. Kang, J. Park, U. Koldemir, J. Suh, D. S. Narang, K. Liu, J. Ji, J. Li, R. Sinclair, and J. Wu, Nano Lett. **14**, 3185 (2014).

[32] X. Zhu, N. R. Monahan, Z. Gong, H. Zhu, K. W. Williams, and C. A. Nelson, J. Am. Chem. Soc. **137**, 8313 (2015).

[33] A. F. Rigosi, H. M. Hill, Y. Li, A. Chernikov, and T. F. Heinz, Nano Lett. **15**, 5033 (2015).

[34] J. Zhang, J. Wang, P. Chen, Y. Sun, S. Wu, Z. Jia, X. Lu, H. Yu, W. Chen, J. Zhu, G. Xie, R. Yang, D. Shi, X. Xu, J. Xiang, K. Liu, and G. Zhang, Adv. Mater. **28**, 1950 (2016).

[35] H. M. Hill, A. F. Rigosi, K. T. Rim, G. W. Flynn, and T. F. Heinz, Nano Lett. **16**, 4831 (2016).

[36] M. M. Furchi, F. Höller, L. Dobusch, D. K. Polyushkin, S. Schuler, and T. Mueller, npj 2D Mater. Appl. **2**, 3 (2018).

[37] P. Rivera, J. R. Schaibley, A. M. Jones, J. S. Ross, S. Wu, G. Aivazian, P. Klement, K. Seyler, G. Clark, N. J. Ghimire, J. Yan, D. G. Mandrus, W. Yao, and X. Xu, Nat. Commun. **6**, 6242 (2015).

[38] F. Wu, T. Lovorn, and A. H. MacDonald, Phys. Rev. B **97**, 035306 (2018).

[39] N. Zibouche, A. Kuc, J. Musfeldt, and T. Heine, Ann. Phys. **526**, 395 (2014).

[40] N. R. Wilson, P. V. Nguyen, K. Seyler, P. Rivera, A. J. Marsden, Z. P. L. Laker, G. C. Constantinescu, V. Kandyba, A. Barinov, N. D. M. Hine, X. Xu, and D. H. Cobden, Sci. Adv. **3**, e1601832 (2017).

[41] G. Strinati, Phys. Rev. Lett. **49**, 1519 (1982).

[42] M. Rohlfing and S. G. Louie, Phys. Rev. B **62**, 4927 (2000).

[43] M. Palummo, O. Pulci, R. D. Sole, A. Marini, P. Hahn, W. G. Schmidt, and F. Bechstedt, J. Phys.: Condens. Matter **16**, S4313 (2004).

[44] P. Giannozzi, S. Baroni, N. Bonini, M. Calandra, R. Car, C. Cavazzoni, D. Ceresoli, G. L. Chiarotti, M. Cococcioni, I. Dabo, A. Dal Corso, S. de Gironcoli, S. Fabris, G. Fratesi, R. Gebauer, U. Gerstmann, C. Gougoussis, A. Kokalj, M. Lazzeri, L. Martin-Samos, N. Marzari, F. Mauri, R. Mazzarello, S. Paolini, A. Pasquarello, L. Paulatto, C. Sbraccia, S. Scandolo, G. Sclauzero, A. P. Seitsonen, A. Smogunov, P. Umari, and R. M. Wentzcovitch, J. Phys.: Condens. Matter **21**, 395502 (19pp) (2009).

[45] D. R. Hamann, Phys. Rev. B **88**, 085117 (2013).

[46] M. J. van Setten, M. Giantomassi, E. Bousquet, M. J. Verstraete, D. R. Hamann, X. Gonze, and G.-M Rignanese, Comput. Phys. Commun. **226**, 39 (2018).

[47] L. Hedin and S. Lundqvist, Solid State Phys. **23**, 1 (1970).

[48] G. Onida, L. Reining, and A. Rubio, Rev. Mod. Phys. **74**, 601 (2002).

[49] A. Marini, C. Hogan, M. Grüning, and D. Varsano, Comput. Phys. Commun. **180**, 1392 (2009).

[50] A. Molina-Sánchez, D. Sangalli, K. Hummer, A. Marini, and L. Wirtz, Phys. Rev. B **88**, 045412 (2013).

[51] A. Molina-Sánchez, K. Hummer, and L. Wirtz, Surf. Sci. Rep. **70**, 554 (2015).

[52] D. Y. Qiu, F. H. da Jornada, and S. G. Louie, Phys. Rev. Lett. **111**, 216805 (2013).

[53] Y. Yu, S. Hu, L. Su, L. Huang, Y. Liu, Z. Jin, A. A. Purezky, D. B. Geohegan, K. W. Kim, Y. Zhang, and L. Cao, Nano Lett. **15**, 486 (2015).

[54] A. V. Kolobov and J. Tominaga, *Two-Dimensional Transition-Metal Dichalcogenides*, Springer Series in Materials Science (Springer International Publishing, Switzerland, 2016).

[55] J. P. Echeverry, B. Urbaszek, T. Amand, X. Marie, and I. C. Gerber, Phys. Rev. B **93**, 121107 (2016).

[56] In order to diagonalize the Bethe-Salpeter Hamiltonian and obtain the wave functions of the first excitonic states we implemented a new diagonalization mode in the Yambo code using the SLEPc library (http://slepc.upv.es/). This library provides iterative algorithms to obtain the N lowest energy eigenvalues and corresponding eigenvectors in a selected energy range.

[57] F. Paleari, T. Galvani, H. Amara, F. Ducastelle, A. Molina-Sanchez, and L. Wirtz, arXiv:1803.00982.

[58] X.-X. Zhang, Y. You, Shu Yang Frank Zhao, and T. F. Heinz, Phys. Rev. Lett. **115**, 257403 (2015).

[59] M. Palummo, M. Bernardi, and J. C. Grossman, Nano Lett. **15**, 2794 (2015).

[60] W. van Roosbroeck and W. Shockley, Phys. Rev. **94**, 1558 (1954).

[61] A. Molina-Sánchez, M. Palummo, A. Marini, and L. Wirtz, Phys. Rev. B **93**, 155435 (2016).

[62] Pedro Miguel M. C. de Melo and A. Marini, Phys. Rev. B **93**, 155102 (2016).

[63] S. Gao, L. Yang, and C. D. Spataru, Nano Lett. **17**, 7809 (2017).

[64] R. Gillen and J. Maultzsch, Phys. Rev. B **97**, 165306 (2018).

[65] T. Deilmann and K. S. Thygesen, Nano Lett. **18**, 1460 (2018).

[66] S. Varrette, P. Bouvry, H. Cartiaux, and F. Georgatos, in *Proceedings of the 2014 International Conference on High Performance Computing & Simulation (HPCS 2014)* (IEEE, Bologna, Italy, 2014), pp. 959–967.